ACS APPLIED MATERIALS & INTERFACES

www.acsami.org

Research Article

KCl-Mediated Defect Passivation in Vapor-Deposited Perovskites

Vladimir Held,* Nada Mrkyvkova,* Yuriy Halahovets, Peter Nádaždy, Karol Vegso, Aleš Vlk, Martin Ledinský, Andrei Chumakov, Matthias Schwartzkopf, Frank Schreiber, and Peter Siffalovic

Cite This: *ACS Appl. Mater. Interfaces* 2025, 17, 43877−43884

Read Online

ACCESS | Metrics & More | Article Recommendations | Supporting Information

ABSTRACT: Perovskite-based solar cells (PSCs) have reached efficiencies comparable to those of commonly used silicon solar panels. Despite the promise of PSCs, their efficiency and commercial viability are currently restricted by three main factors: nonradiative charge recombinations on defects occurring within the light-absorbing layer and at its boundaries, limited reproducibility, and upscaling due to widely employed wet deposition methods. To address these issues, we investigated the defect passivation strategy by introducing potassium salt (KCl) during perovskite vapor deposition. We observed effective passivation of the defects upon KCl addition, manifested as an immediate and significant enhancement of the real-time photoluminescence (PL) intensity. The efficiency of passivation is related to the ionic nature of the potassium salt and its flux density. On the other hand, the perovskite's crystallographic structure and texture, as observed from the grazing-incidence wide/small-angle X-ray scattering measurements, showed no significant changes due to KCl doping. Our work provides valuable insight into the possible passivation routes for the vapor-deposited perovskite layers, with implications for various chemical compositions or architectures.

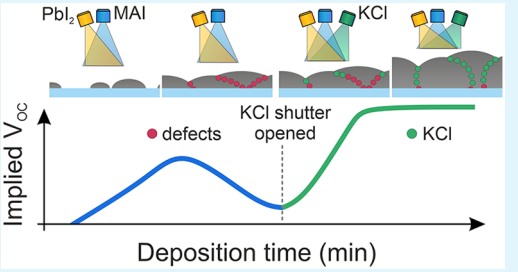

KEYWORDS: *Lead-halide perovskite, vapor deposition, defect passivation, potassium salts, growth kinetics*

INTRODUCTION

Metal-halide perovskites represent a promising material for solar cells, demonstrating remarkable efficiencies that, in some cases, exceed those of well-established silicon-based solar cells.[1] This has prompted intense research into their fundamental properties and potential for commercialization.[2−6] Their integration into tandem solar cells—either as pure perovskite tandems or in combination with textured silicon bottom cells—unlocks promising avenues for exceeding the efficiency limits of conventional photovoltaic (PV) technologies.[1,7−9] Despite the high efficiencies achieved in perovskite-based PV, further advancements are limited by high defect densities throughout the perovskite layer, including the bulk, grain boundaries, and interfaces.[10−13] These defects, primarily antisites, vacancies, and interstitial point defects, typically promote nonradiative charge recombinations, reducing the open-circuit voltage (V_{OC}) of the solar cell and, thus, its overall performance. Therefore, minimizing these defects across all regions of the perovskite film is essential for continued progress.

Numerous passivation strategies have been implemented to minimize defect densities and suppress nonradiative charge recombinations. These strategies, especially explored for wet deposition techniques, include the direct addition of functional agents, such as small molecules, fullerenes, polymers, PbI_2, zwitterions, nanoparticles, and ammonium or alkali salts into the perovskite precursor solution.[10,14−16] A positive influence on PV device characteristics has been reported for all of these additives, manifested as improved stability, reduced interfacial recombination, or the elimination of charge accumulation and hysteresis phenomena. Although the concepts of defect passivation have been widely studied and implemented in solution-based methods, their development is significantly lagging in vapor-deposited perovskite devices.

Vapor phase deposition is currently a key industrial technique for optoelectronic thin films, and naturally, it has also been extensively developed and enhanced for perovskite fabrication, despite its greater complexity compared to solution-based methods. Vapor deposition allows the fabrication of large-area and complex multilayer-structure devices based on precise control over film thickness, composition, and reproducibility.[2] Despite its benefits in the commercial segment, defect passivation strategies that would improve the efficiency of PV devices have not been widely studied. Recent work focuses mainly on the interface passivation by the 2D perovskites and alkali metal salts.[17−19] Therefore, further efforts are needed to develop vapor-based passivation strategies for the perovskite layer and its interfaces. Specifically, *in situ* passivation, integrated directly into absorber fabrication,

Received: May 13, 2025
Revised: July 1, 2025
Accepted: July 7, 2025
Published: July 21, 2025

should be prioritized, with the engagement of established knowledge from solution-based passivation techniques.

In this work, we study the effect of KCl doping on the optoelectronic and structural properties during $MAPbI_3$ vacuum co-deposition, employing *in situ* photoluminescence (PL) and grazing-incidence wide/small-angle X-ray scattering (GI-WAXS/SAXS) techniques. The solar cell's performance is directly linked to its PL quantum yield (PLQY), a crucial metric reflecting defect density and the resulting charge carrier collection potential. Therefore, PL monitoring is essential for determining the impact of doping on defect passivation and optoelectronic layer properties. Since the PL intensity reflects the density of defects causing nonradiative recombinations, we will refer to this type of defect specifically in the following text. On the other hand, GIWAXS provides information about the crystalline structure, preferred orientation, and phase purity of the grown film.[20] While researchers commonly rely on a trial-and-error approach to optimize the fabrication process, *in situ* techniques enable direct access to growth dynamics and defect density evolution—key insights that are otherwise inaccessible with conventional *ex situ* methods.

Potassium salt was selected as the most promising alkali metal for defect passivation,[16,21−23] having also been successfully used in vacuum deposition studies recently.[18,19] We observed that the KCl addition leads to instant defect passivation in the perovskite layer, directly proportional to the KCl flux. On the other hand, we did not observe any structural changes in the perovskite—such as new crystallographic or chemical phases—that could be directly attributed to KCl doping. We believe that this *in situ* study provides an important step in developing targeted vapor-based passivation techniques and offers a way to improve the performance and stability of vacuum-deposited perovskite films significantly.

EXPERIMENTAL SECTION

$MAPbI_3$ perovskite with KCl additive was grown by vacuum thermal co-deposition of three precursors—lead iodide (PbI_2), methylammonium iodide (MAI), and potassium chloride (KCl). A custom-made vacuum chamber equipped with two viewports and a 360° cylindrical beryllium (Be) window was used, enabling simultaneous measurement of PL and GIWAXS during the $MAPbI_3$ growth (see Figures S1 and S2 in the Supporting Information).[12,24] The precursors were evaporated from the Knudsen effusion cells on a Si substrate (with native oxide) at a base pressure of approximately 10^{-6} mbar. The deposition chamber was equipped with three separate QCM sensors: two placed close to the MAI and PbI_2 evaporators and one at the substrate level (for KCl) to measure the deposition rate of precursors. We note that the high evaporation temperature of KCl (550 °C) prevented accurate measurement of the deposition rate near the KCl effusion cell due to the malfunction of the QCM sensor. First, the pure $MAPbI_3$ perovskite layer was grown, having only the crucibles with PbI_2 and MAI precursors opened. The temperature of the MAI and PbI_2 crucible was set to 160 and 280 °C, respectively. The KCl precursor was evaporated later during $MAPbI_3$ growth. The control deposition of pentacene (PEN) was performed at a crucible temperature of 160 °C, with an evaporation rate of ∼4 Å/min, monitored by a QCM placed near the PEN crucible. The experiment was conducted at the P03 beamline at PETRAIII synchrotron (DESY, Hamburg, Germany). The energies of the X-ray radiation and the excitation laser for PL were set to 11.85 keV ($\lambda_{X\text{-}ray}$ = 1.048 Å) and 2.33 eV (λ_{PL} = 532 nm), respectively. For a detailed description of the experimental conditions, perovskite evaporation procedure, and setup, see the Supporting Information.

RESULTS AND DISCUSSION

The $MAPbI_3$ layers were prepared using a vapor deposition method, following the experimental procedure described in our previous work.[25] Here, the PbI_2 and MAI powders were heated, and once the evaporation temperature was stabilized, the respective crucible shutter was opened. The precursors were evaporated onto a Si substrate (with native oxide), forming a perovskite film after the shutter above the substrate surface was removed. Once the thin $MAPbI_3$ layer was formed, continuous KCl salt evaporation was introduced. We emphasize that the KCl additive was not applied during the initial perovskite growth phase; it was introduced only after the thin perovskite layer had been grown. This deliberate timing allowed for the precise identification of its effect on the optoelectronic and structural characteristics of the perovskite layer. The influence of KCl on the $MAPbI_3$ properties was investigated by simultaneous measurement of PL and GI-WAXS/SAXS during the entire evaporation process; refer to the schematic illustration of the experimental setup in Figure 1.

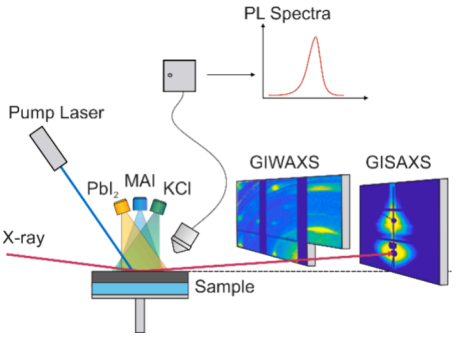

Figure 1. Schematic illustration of $MAPbI_3$ perovskite vacuum deposition and KCl additive with the simultaneous measurement of the photoluminescence and grazing-incidence scattering.

Figure 2a shows the PL spectral evolution measured during the $MAPbI_3$ deposition. The PL spectra were fitted with a

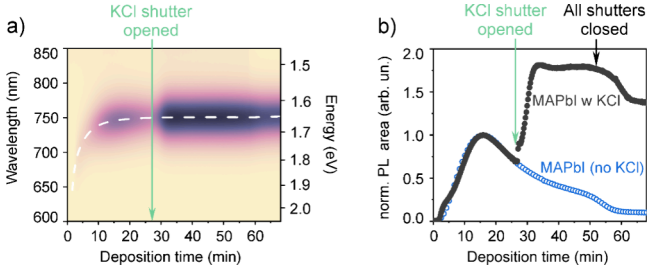

Figure 2. a) Spectrally resolved PL heat map during $MAPbI_3$ growth (excitation laser wavelength was 532 nm). The PL intensity distribution corresponds to wavelengths, and the PL energy scale is only indicative. The white dashed line indicates the PL peak position. b) Temporal evolution of the normalized PL peak intensity during deposition of pure $MAPbI_3$ with no KCl (blue points) and $MAPbI_3$ with KCl addition (black points). The perovskite layer thickness did not exceed 25 nm at the end of the deposition.

Gaussian function, and the obtained PL peak position, corresponding to the effective band gap width, is indicated by the white dashed line. We observed a redshift of the PL peak position with increasing perovskite layer thickness, which aligns with our prior findings and can be explained by quantum

https://doi.org/10.1021/acsami.5c09426
ACS Appl. Mater. Interfaces 2025, 17, 43877−43884

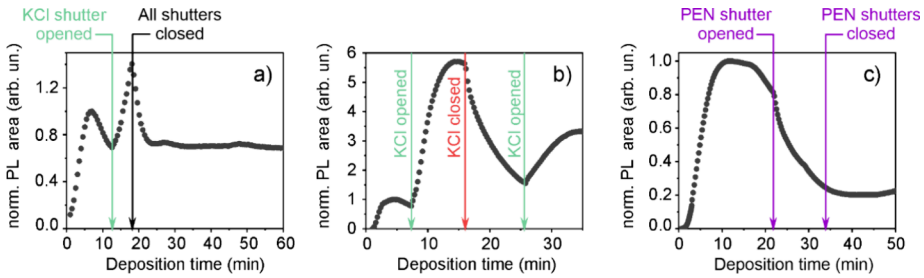

Figure 3. Temporal evolution of the normalized PL peak intensity for $MAPbI_3$ growth with addition of KCl (a,b) and PEN molecules (c).

confinement in the vertical direction of perovskite islands during the early stages of growth.[12,13,26−31] Importantly, the KCl additive did not influence the band gap width ∼1.65 eV, being a typical value for thermally evaporated thin-film $MAPbI_3$ perovskite.[32−36] On the other hand, KCl had a clear impact on the PL intensity temporal profile.

Figure 2b shows the normalized PL peak area for two distinct $MAPbI_3$ depositions—with and without KCl evaporation (black and blue points, respectively). The PL intensity evolution of pure $MAPbI_3$ with no additives was rescaled in time to match the temporal PL evolution of $MAPbI_3$ with KCl. A detailed analysis of the PL intensity evolution of pure $MAPbI_3$ during vacuum deposition was thoroughly described in our previous work in ref 13. The initial increase in the emission intensity is assigned to the growth of the individual perovskite grains until the coalescence occurs.[24] The subsequent PL quenching is caused by defect formation at the grain boundaries, which increases proportionally with the deposition time. Interestingly, the PL intensity evolution trend seems universal for different deposition methods and perovskite compositions.[12,27,30,31,37,38]

To directly examine the passivation effect of KCl, the $MAPbI_3$ layer was grown up to the point where the PL intensity started to quench. Here, the individual perovskite grains (nanocrystallites) coalesce into a continuous layer, forming common grain boundaries. The increasing surface of the grain boundaries during the perovskite growth represents increasing defect density, resulting in PL intensity quenching. At this point, the KCl shutter was opened. The PL intensity recovered instantly, and after ∼5 min of KCl deposition, it almost doubled its maximal value reached at the point of grain coalescence. The immediate increase in PL intensity suggests a passivation of the defects by KCl. Based on repeated depositions under similar conditions, we observe PL intensity increase by a factor of 2 (±0.3). The emission intensity increases after potassium salt addition, either in the steady-state PL spectra or in the time-resolved PL measurements, as reported previously in refs 18, 19, 21, and 23. However, the dynamics of the passivation process during the perovskite layer formation have not yet been reported yet.

The fact that the PL intensity surpassed its maximal value (during the dominant grain coalescence period) indicates that KCl effectively passivates defects at the grain boundaries. The emission intensity stabilizes during further perovskite deposition, although the thickness of the perovskite layer increases. We note that the layer thickness growth rate is slowed down after KCl introduction due to the increased temperature of the layer surface, as shown in Figure S4 and discussed later in the manuscript. However, the PL intensity saturation is not caused by a limited penetration depth. The PL signal is generated from the whole depth of the $MAPbI_3$ layer, as the layer thickness does not exceed the penetration depth of the excitation laser during the entire deposition process (the penetration depth for the used excitation wavelength of 532 nm is ∼120 nm,[39,40] and the perovskite layer thickness at the end of the deposition did not exceed 25 nm). Therefore, the density of photoexcited charge carriers in the film and, consequently, the PL intensity should naturally increase with film thickness, provided that defects during growth are well passivated. For the observed PL saturation, we can only speculate that the KCl flux was insufficient to effectively passivate the additional perovskite material, as discussed later.

In principle, KCl evaporation enables the in situ passivation of the perovskite layer during growth, allowing for the effective passivation of defects at grain boundaries that might otherwise remain inaccessible to postdeposition treatments. The measured PL intensity allows for estimating the implied V_{OC}, as the PL intensity is directly proportional to the photoluminescence quantum yield PLQY(t).[12] The addition of KCl leads to a significant enhancement in the implied V_{OC}, with improvements of up to 75 mV. The implied V_{OC} is the only parameter that can be further optimized in the perovskite layers, as the short-circuit current J_{SC} is saturated for the formed layer thickness (typically of a few hundred nanometers), and the fill factor (FF) reflects mainly the contact feasibility.[41] Maximized PL intensity indicates minimal nonradiative losses, leading to a larger quasi-Fermi level splitting and, consequently, a higher V_{OC}. Increased V_{OC} and efficient charge extraction facilitated by fewer defects contribute significantly to a higher overall power conversion efficiency (PCE) of perovskite solar cells. Similarly, in the context of light-emitting diodes (LEDs), a higher PL signal—and thus the PLQY—signifies efficient radiative recombination within the material and hence bright and efficient perovskite-based LEDs. Clearly, maximizing the PL intensity is the main goal in perovskite layer fabrication. The passivation of defects, leading to the V_{OC} increase, is easily controllable by the presented approach, facilitating simple optimization of a combined deposition−passivation process for the fabrication of high-quality perovskite thin films.

Finally, we observed a slight emission decrease after all shutters of the precursors were closed—MAI, PbI_2, and KCl shutters. Such a PL intensity drop after the perovskite growth interruption was consistently observed in other depositions, e.g., in Figure 3a. We suppose that the slight decrease in PL intensity may result from temperature changes induced by closing the KCl shutter, which reduces heating from thermal radiation. Nevertheless, the KCl addition resulted in an overall greater PL intensity than it would have been in its absence—see the PL signal from the nonpassivated layer in Figure 2b, where the intensity drops to ∼10% from its maximal value.

https://doi.org/10.1021/acsami.5c09426
ACS Appl. Mater. Interfaces 2025, 17, 43877−43884

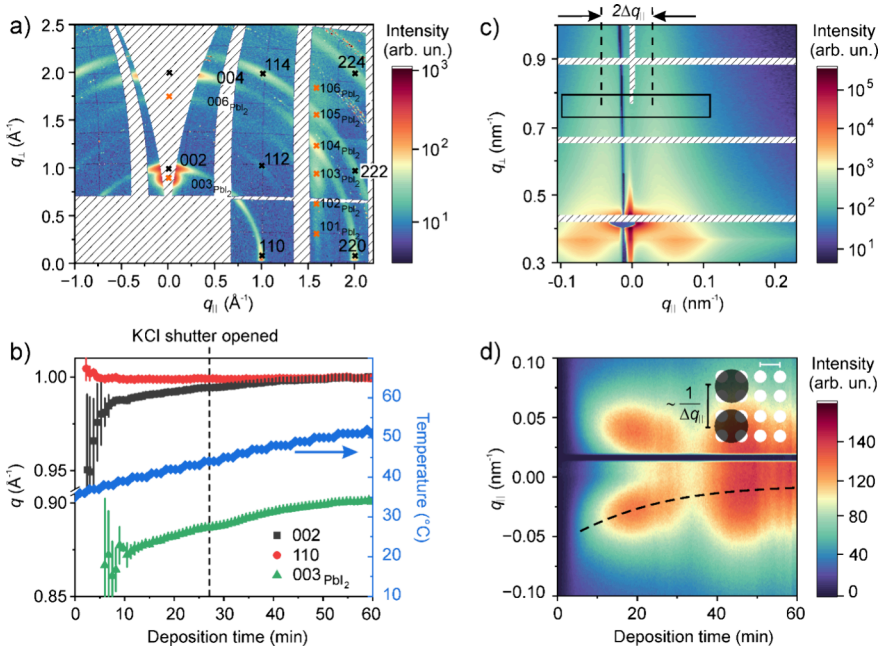

Figure 4. a) GIWAXS pattern of $MAPbI_3$ perovskite immediately following KCl deposition. The calculated positions of the selected diffractions for $MAPbI_3$ (black cross) and PbI_2 (orange cross) are indicated. b) Temporal evolution of the $MAPbI_3$ (002 and 110) and PbI_2 (003) diffraction peak positions during the perovskite deposition, along with the substrate temperature. c) GISAXS pattern. The out-of-plane scattering peaks at a distance of $2\Delta q_\parallel$, indicated by black dashed lines, inversely correspond to the average perovskite island spacing. d) Diffuse scattering along the $q_\parallel$ direction during $MAPbI_3$ layer deposition, obtained by integrating the scattering signal in the black rectangle shown in c). The dashed black line tracks the continuous shift of the out-of-plane scattering peaks toward lower q-values, corresponding to a growth-related increase in the average distance between perovskite islands (see inset).

Figure 3a shows that the KCl additive prevented the emission from dropping below ~70% of its maximal value.

To further support the passivation effect of KCl, we opened the KCl shutter repeatedly during the $MAPbI_3$ deposition, as demonstrated in Figure 3b (see also Figure S3 in the Supporting Information). Additionally, the KCl evaporation rate was increased by a factor of ~3. We note that the deposition rates for PbI_2 and MAI were monitored by quartz crystal microbalances (QCM) placed in the vicinity of each crucible. For KCl, real-time rate monitoring with the QCM placed near the crucible was not possible due to the high evaporation temperature (~550 °C), which caused the QCM to malfunction. Therefore, the exact deposition rate of KCl could not be determined, and it can only be deduced from the preceding rate calibration with the QCM placed at the sample level (approximately 20 cm above the KCl crucible). Figure 3b shows that the increased KCl flux improves the PL emission intensity, surpassing its maximum at the moment of coalescence by almost six times. Closing the KCl shutter leads to gradual PL quenching, which can be explained by the ongoing growth of the perovskite layer containing defects. Subsequent KCl addition restores the PL intensity, but the emission has not fully recovered, indicating that some defects cannot be accessed, or the defect density exceeds the KCl amount. This indicates that sequential passivation is not optimal for achieving maximal PL intensity, highlighting the necessity of continuous passivation under carefully tuned conditions. Nevertheless, perovskite emission recovery, which is directly connected to KCl doping, can be unambiguously linked to the defect passivation effect.

The effect of potassium-based compounds on defect passivation in perovskites has been studied in numerous works, although the exact mechanism of K^+ incorporation is still debated.[18,19,21,22,42−44] We propose that the polar nature of KCl acts as a dual-site passivator, where the ions (K^+ and Cl^-) interact electrostatically with the charged defects, similar to bifunctional additives predominantly utilized in the wet perovskite deposition methods.[11,45,46] The potassium cation might be bound to uncoordinated I (iodine interstitial), MA^+, or the Pb^{2+} vacancies, whereas the chloride anion might interact with the iodide vacancies or the uncoordinated Pb cations.[22,42,43,45] The defect passivation with potassium salts during perovskite vapor deposition is straightforward, as the evaporation of pure potassium metal is challenging due to its low melting point, high reactivity in air, and tendency to form compounds. Moreover, there is strong collective evidence that a small amount of Cl dopants facilitates the formation of larger perovskite grains while simultaneously reducing defect densities at the grain boundaries.[47−53] To contrast and confirm the beneficial role of polar molecules in perovskite passivation, we also evaporated pentacene (PEN), a molecule with a negligible dipole moment, during $MAPbI_3$ growth. Figure 3c shows that PEN addition had no passivation effect on the PL intensity, as expected. The PL signal was quenched as it typically is after the perovskite crystallite coalescence, without any significant influence of PEN molecules on the emission progression. These data manifest the importance of the ions in the passivation process of the perovskite thin films.

In the following section, we discuss the impact of KCl on the crystallographic structure and morphology of the perovskite film during growth. Figure 4a shows the GIWAXS reciprocal space map, reflecting the crystallographic structure of the $MAPbI_3$ layer 3 min after KCl deposition was initiated. The diffraction peak positions indicate a tetragonal structure commonly observed for $MAPbI_3$ films at temperatures below the cubic-phase transition point at $T = (55 \pm 5)$ °C.[54−56]

https://doi.org/10.1021/acsami.5c09426
ACS Appl. Mater. Interfaces 2025, 17, 43877−43884

These observations are consistent with our previous findings on the crystallographic structure of $MAPbI_3$ grown by vacuum deposition.[57] Along with the perovskite phase, a PbI_2 phase with an unusual symmetry is also visible (unit cell parameters: $a \sim 4.55$ Å^{-1}, $b \sim 4.55$ Å^{-1}, $c \sim 21.05$ Å^{-1}, $\alpha = 90°$, $\beta = 90°$, and $\gamma = 120°$).[58−60] We note that such a PbI_2 phase may be, in fact, common in perovskite layers, but its precise crystallographic structure is often not the primary focus of the study. Figure 4b shows the temporal evolution of $MAPbI_3$ and PbI_2 selected diffractions during perovskite growth. In the case of $MAPbI_3$, we observe a continuous shift of the 002 diffraction peak position in the reciprocal space toward the 110 reflection, indicating the gradual change from the tetragonal to cubic phase (the evolution of the diffraction intensities and widths is shown in Figures S4 and S5, together with the GIWAXS reciprocal map at the end of the deposition in Figure S6). Such continuous phase transformation cannot be attributed to the sudden introduction of the KCl compound in the perovskite layer, and other factors need to be examined.

The KCl salt is evaporated at high temperatures (550 °C), which significantly exceeds the deposition temperatures of PbI_2 and MAI precursors at 280 and 160 °C, respectively. The high temperature of the KCl crucible causes the substrate, i.e., the perovskite layer, heating via thermal radiation, as shown in Figure 4b (see also the schematic indication in Figure S1 in the Supporting Information). The increasing substrate temperature leads to the continuous change of the perovskite unit cell parameters until the cubic phase is finally reached near the phase transition temperature. We note that the substrate temperature was measured by a thermocouple attached to a plate below the substrate. The actual temperature at the perovskite surface is $\sim(5 \pm 2)$ °C higher. The increased substrate temperature likely promotes the presence of the PbI_2 phase in the early stages of the perovskite growth, with its further accumulation with a gradual temperature increase during the deposition; see Figure S4 in the Supporting Information. Notably, we did not observe any PbI_2 excess in the perovskite layer under similar deposition conditions without KCl addition, when the substrate temperature did not exceed 40 °C.[13] The increasing substrate temperature and the subsequent gradual PbI_2 phase excess might have a positive effect on the defect passivation, as previously reported in refs 10, 61, and 62. Such defect passivation was primarily attributed to the occurrence or increase of the PbI_2 phase because, in general, $MAPbI_3$ films exhibit a decrease in PL intensity with increasing temperature, regardless of their crystallographic phase.[63−65] Overall, the continuous rise in the substrate temperature cannot account for the abrupt increase in PL intensity observed after the introduction of KCl, which we associate with defect passivation in the perovskite layer. The enhancement in PL is rapid and pronounced, occurring on a much shorter time scale than the gradual thermal effects. Additionally, the temporal profile of the PL intensity following KCl introduction changes too quickly to be explained by the slow and progressive increase in the PbI_2 phase (or the continuous change of the perovskite crystal structure), which evolves more gradually during the deposition process. This discrepancy in time scales further supports our interpretation that the PL increase is primarily driven by the chemical interaction between KCl and the perovskite rather than by thermal effects or structural transformations involving PbI_2.

Figure 4c shows the GISAXS diffraction map, reflecting the surface morphology after ∼6 min of deposition. Here, the diffuse out-of-plane scattering (peaks highlighted by black dashed lines) indicates laterally correlated perovskite islands at the early stages of the deposition. The scattering peak distance $2\Delta q_{\parallel}$ inversely corresponds to the average spacing distribution between perovskite islands $D \approx 2\pi/\Delta q_{\parallel}$.[66−68] The temporal evolution of the peak distance in the reciprocal space, obtained by integrating the scattering intensity in the range of $q_{\perp} \sim 0.7-0.8$ nm^{-1} (see black rectangle in Figure 4c), is shown in Figure 4d. We observe a continuous shift of the scattering peak position from larger to smaller $q_{\parallel}$ values with the deposition progress. The observed shift in the out-of-plane peak can be attributed to the increasing mean distance between nanostructures as a consequence of island coalescence and subsequent size growth, depicted schematically in the inset of Figure 4d. We note that island coalescence behavior in vacuum-deposited hybrid perovskite differs from that of more conventional inorganic materials, where nanocluster coalescence yields a relatively uniform layer.[68] Instead, perovskites form mounded surfaces, making it difficult to identify the exact moment of coalescence using GISAXS analysis.[13]

Interestingly, the KCl introduction at the 27th minute of the perovskite growth did not produce any observable changes in the GISAXS patterns. The decrease in the out-of-plane scattering intensity at ∼33 min is caused by the growing layer thickness, translating into periodic constructive and destructive changes in the scattering intensity.[13] Overall, we can conclude that KCl addition did not induce any substantial modifications of the perovskite crystallographic structure. The major tetragonal to cubic phase transition is due to the gradual temperature increase caused by heat radiation from the KCl crucible.

CONCLUSION

In conclusion, we employed a novel *in situ* measurement approach, combining PL spectroscopy and grazing-incidence wide/small-angle X-ray scattering (GIWAXS/SAXS), to investigate the impact of KCl addition on the optoelectronic and structural characteristics of the $MAPbI_3$ perovskite during vapor deposition. Our findings reveal an immediate and significant enhancement of the PL intensity upon introducing KCl salt, indicating efficient passivation of defects in the perovskite layer—especially at the grain boundaries. This approach leads to a notable enhancement in the implied V_{OC}, with an up to 75 mV improvement. Control experiments with pentacene evaporation showed no such PL enhancement, highlighting the importance of the ionic nature of KCl for defect passivation. Notably, while KCl significantly enhanced the PL intensity, GI-WAXS/SAXS measurements showed no substantial alterations in the perovskite's crystallographic structure that could be directly attributed to KCl doping. Instead, a gradual tetragonal-to-cubic phase transition was observed, primarily driven by heating the perovskite layer due to the high temperature of the KCl crucible. Our *in situ* study provides direct evidence for an effective route for defect passivation in perovskite layers by the potassium salt during vacuum deposition, offering valuable insights for optimizing the quality of the absorption layer in the perovskite-based solar cells.

ASSOCIATED CONTENT

Supporting Information

The Supporting Information is available free of charge at https://pubs.acs.org/doi/10.1021/acsami.5c09426.

https://doi.org/10.1021/acsami.5c09426
ACS Appl. Mater. Interfaces 2025, 17, 43877−43884

A detailed description of the $MAPbI_3$ with KCl deposition, experimental conditions, and setup; details on the GIWAXS measurements and analysis; AFM measurements (PDF)

AUTHOR INFORMATION

Corresponding Authors

Vladimir Held − *Institute of Physics, Slovak Academy of Sciences, 845 11 Bratislava, Slovakia;* orcid.org/0000-0003-2210-8285; Email: vladimir.held@uv.es

Nada Mrkyvkova − *Institute of Physics, Slovak Academy of Sciences, 845 11 Bratislava, Slovakia; Center for Advanced Materials Application, Slovak Academy of Sciences, 845 11 Bratislava, Slovakia;* orcid.org/0000-0002-2619-0872; Email: nada.mrkyvkova@savba.sk

Authors

Yuriy Halahovets − *Institute of Physics, Slovak Academy of Sciences, 845 11 Bratislava, Slovakia; Center for Advanced Materials Application, Slovak Academy of Sciences, 845 11 Bratislava, Slovakia;* orcid.org/0000-0002-9269-5705

Peter Nádaždy − *Institute of Physics, Slovak Academy of Sciences, 845 11 Bratislava, Slovakia; Institute of Electrical Engineering, Slovak Academy of Sciences, 845 11 Bratislava, Slovakia*

Karol Vegso − *Institute of Physics, Slovak Academy of Sciences, 845 11 Bratislava, Slovakia; Center for Advanced Materials Application, Slovak Academy of Sciences, 845 11 Bratislava, Slovakia;* orcid.org/0000-0003-2595-6036

Aleš Vlk − *Laboratory of Thin Films, Institute of Physics, ASCR, 162 00 Prague, Czech Republic;* orcid.org/0000-0003-2866-7133

Martin Ledinský − *Laboratory of Thin Films, Institute of Physics, ASCR, 162 00 Prague, Czech Republic;* orcid.org/0000-0002-6586-5473

Andrei Chumakov − *Photon Science, Deutsches Elektronen-Synchrotron (DESY), 22607 Hamburg, Germany;* orcid.org/0000-0003-3195-9356

Matthias Schwartzkopf − *Photon Science, Deutsches Elektronen-Synchrotron (DESY), 22607 Hamburg, Germany;* orcid.org/0000-0002-2115-9286

Frank Schreiber − *Institute of Applied Physics, University of Tübingen, 72076 Tübingen, Germany;* orcid.org/0000-0003-3659-6718

Peter Siffalovic − *Institute of Physics, Slovak Academy of Sciences, 845 11 Bratislava, Slovakia; Center for Advanced Materials Application, Slovak Academy of Sciences, 845 11 Bratislava, Slovakia;* orcid.org/0000-0002-9807-0810

Complete contact information is available at: https://pubs.acs.org/10.1021/acsami.5c09426

Notes

The authors declare no competing financial interest.

ACKNOWLEDGMENTS

We acknowledge the financial support of projects IMPULZ (IM-2023-82), APVV-21-0297, APVV-20-0111, SK-CZ-RD-21-0043, 2023/727/PVKSC, and ITMS project code 313021T081. The authors also acknowledge the support of the BMBF, DFG, and projects LUASK 22202 and PVKSC 9F23003. We acknowledge DESY (Hamburg, Germany), a member of the Helmholtz Association HGF, for the provision of experimental facilities. Parts of this research were carried out at P03 beamline of PETRA III light source. The authors further acknowledge the OSCARS project, which has received funding from the European Commission's Horizon Europe Research and Innovation program under Grant Agreement No. 101129751.

REFERENCES

(1) National Renewable Energy Laboratory (NREL). Best Research-Cell Efficiency Chart. 2025. https://www.nrel.gov/pv/cell-efficiency.html.

(2) Abzieher, T.; Moore, D. T.; Roß, M.; Albrecht, S.; Silvia, J.; Tan, H.; Jeangros, Q.; Ballif, C.; Hoerantner, M. T.; Kim, B. S.; Bolink, H. J.; Pistor, P.; Goldschmidt, J. C.; Chiang, Y. H.; Stranks, S. D.; Borchert, J.; McGehee, M. D.; Morales-Masis, M.; Patel, J. B.; Bruno, A.; Paetzold, U. W. Vapor Phase Deposition of Perovskite Photovoltaics: Short Track to Commercialization? *Energy Environ. Sci.* **2024**, *17* (5), 1645−1663.

(3) Snaith, H. J. Present Status and Future Prospects of Perovskite Photovoltaics. *Nat. Mater.* **2018**, *17* (5), 372−376.

(4) Correa-Baena, J. P.; Saliba, M.; Buonassisi, T.; Grätzel, M.; Abate, A.; Tress, W.; Hagfeldt, A. Promises and Challenges of Perovskite Solar Cells. *Science* **2017**, *358* (6364), 739−744.

(5) Cheng, Y.; Ding, L. Pushing Commercialization of Perovskite Solar Cells by Improving Their Intrinsic Stability. *Energy Environ. Sci.* **2021**, *14* (6), 3233−3255.

(6) Moody, N.; Sesena, S.; deQuilettes, D. W.; Dou, B. D.; Swartwout, R.; Buchman, J. T.; Johnson, A.; Eze, U.; Brenes, R.; Johnston, M.; Haynes, C. L.; Bulović, V.; Bawendi, M. G. Assessing the Regulatory Requirements of Lead-Based Perovskite Photovoltaics. *Joule* **2020**, *4* (5), 970−974.

(7) Chiang, Y. H.; Frohna, K.; Salway, H.; Abfalterer, A.; Pan, L.; Roose, B.; Anaya, M.; Stranks, S. D. Vacuum-Deposited Wide-Bandgap Perovskite for All-Perovskite Tandem Solar Cells. *ACS Energy Lett.* **2023**, *8* (6), 2728−2737.

(8) Chin, X. Y.; Turkay, D.; Steele, J. A.; Tabean, S.; Eswara, S.; Mensi, M.; Fiala, P.; Wolff, C. M.; Paracchino, A.; Artuk, K.; Jacobs, D.; Guesnay, Q.; Sahli, F.; Andreatta, G.; Boccard, M.; Jeangros, Q.; Ballif, C. Interface Passivation for 31.25%-Efficient Perovskite/Silicon Tandem Solar Cells. *Science* **2023**, *381* (6653), 59−63.

(9) Mao, L.; Yang, T.; Zhang, H.; Shi, J.; Hu, Y.; Zeng, P.; Li, F.; Gong, J.; Fang, X.; Sun, Y.; Liu, X.; Du, J.; Han, A.; Zhang, L.; Liu, W.; Meng, F.; Cui, X.; Liu, Z.; Liu, M. Fully Textured, Production-Line Compatible Monolithic Perovskite/Silicon Tandem Solar Cells Approaching 29% Efficiency. *Adv. Mater.* **2022**, *34* (40), 1−12.

(10) Byranvand, M. M.; Saliba, M. Defect Passivation of Perovskite Films for Highly Efficient and Stable Solar Cells. *Solar RRL* **2021**, *5* (8), 2100295.

(11) Shen, X.; Kang, K.; Yu, Z.; Jeong, W. H.; Choi, H.; Park, S. H.; Stranks, S. D.; Snaith, H. J.; Friend, R. H.; Lee, B. R. Passivation Strategies for Mitigating Defect Challenges in Halide Perovskite Light-Emitting Diodes. *Joule* **2023**, *7* (2), 272−308.

(12) Mrkyvkova, N.; Held, V.; Nádaždy, P.; Subair, R.; Majkova, E.; Jergel, M.; Vlk, A.; Ledinsky, M.; Kotlár, M.; Tian, J.; Siffalovic, P. Combined in Situ Photoluminescence and X-Ray Scattering Reveals Defect Formation in Lead-Halide Perovskite Films. *J. Phys. Chem. Lett.* **2021**, *12* (41), 10156−10162.

(13) Held, V.; Mrkyvkova, N.; Nadazdy, P.; Vegso, K.; Vlk, A.; Ledinsky, M.; Jergel, M.; Chumakov, A.; Roth, S. V.; Schreiber, F.; Siffalovic, P. Evolution of Structure and Optoelectronic Properties During Halide Perovskite Vapor Deposition. *J. Phys. Chem. Lett.* **2022**, *13*, 11905.

(14) Ye, J.; Byranvand, M. M.; Martínez, C. O.; Hoye, R. L. Z.; Saliba, M.; Polavarapu, L. Defect Passivation in Lead-Halide Perovskite Nanocrystals and Thin Films: Toward Efficient LEDs and Solar Cells. *Angewandte Chemie - International Edition* **2021**, *60* (40), 21636−21660.

(15) Zhang, F.; Zhu, K. Additive Engineering for Efficient and Stable Perovskite Solar Cells. *Adv. Energy Mater.* **2020**, *10* (13), 1−26.
(16) Tang, Z.; Uchida, S.; Bessho, T.; Kinoshita, T.; Wang, H.; Awai, F.; Jono, R.; Maitani, M. M.; Nakazaki, J.; Kubo, T.; Segawa, H. Modulations of Various Alkali Metal Cations on Organometal Halide Perovskites and Their Influence on Photovoltaic Performance. *Nano Energy* **2018**, *45*, 184−192.
(17) La-Placa, M. G.; Gil-Escrig, L.; Guo, D.; Palazon, F.; Savenije, T. J.; Sessolo, M.; Bolink, H. J. Vacuum-Deposited 2D/3D Perovskite Heterojunctions. *ACS Energy Lett.* **2019**, *4* (12), 2893−2901.
(18) Zhang, S.; Yan, X.; Liu, Z.; Zhu, H.; Yang, Z.; Huang, Y.; Liu, S.; Wu, D.; Pan, M.; Chen, W. Evaporated Potassium Chloride for Double-Sided Interfacial Passivation in Inverted Planar Perovskite Solar Cells. *Journal of Energy Chemistry* **2021**, *54*, 493−500.
(19) Jiang, X.; Geng, C.; Yu, X.; Pan, J.; Zheng, H.; Liang, C.; Li, B.; Long, F.; Han, L.; Cheng, Y. B.; Peng, Y. Doping with KBr to Achieve High-Performance CsPbBr3 Semitransparent Perovskite Solar Cells. *ACS Appl. Mater. Interfaces* **2024**, *16* (15), 19039−19047.
(20) Grishko, A. Y.; Komkova, M. A.; Marchenko, E. I.; Chumakova, A. V.; Tarasov, A. B.; Goodilin, E. A.; Eliseev, A. A. Evidence for Polarization-Induced Phase Transformations and Degradation in CH3NH3PbI3. *Nano Res.* **2023**, *16* (7), 9435−9442.
(21) Abdi-Jalebi, M.; Andaji-Garmaroudi, Z.; Cacovich, S.; Stavrakas, C.; Philippe, B.; Richter, J. M.; Alsari, M.; Booker, E. P.; Hutter, E. M.; Pearson, A. J.; Lilliu, S.; Savenije, T. J.; Rensmo, H.; Divitini, G.; Ducati, C.; Friend, R. H.; Stranks, S. D. Maximizing and Stabilizing Luminescence from Halide Perovskites with Potassium Passivation. *Nature* **2018**, *555* (7697), 497−501.
(22) Son, D. Y.; Kim, S. G.; Seo, J. Y.; Lee, S. H.; Shin, H.; Lee, D.; Park, N. G. Universal Approach toward Hysteresis-Free Perovskite Solar Cell via Defect Engineering. *J. Am. Chem. Soc.* **2018**, *140* (4), 1358−1364.
(23) Azmi, R.; Nurrosyid, N.; Lee, S. H.; Al Mubarok, M.; Lee, W.; Hwang, S.; Yin, W.; Ahn, T. K.; Kim, T. W.; Ryu, D. Y.; Do, Y. R.; Jang, S. Y. Shallow and Deep Trap State Passivation for Low-Temperature Processed Perovskite Solar Cells. *ACS Energy Lett.* **2020**, *5* (5), 1396−1403.
(24) Held, V.; Mrkyvkova, N.; Halahovets, Y.; Nádaždy, P.; Vegso, K.; Vlk, A.; Ledinský, M.; Jergel, M.; Bernstorff, S.; Keckes, J.; Schreiber, F.; Siffalovic, P. Evolution of Defects, Morphology, and Strain during FAMAPbI3 Perovskite Vacuum Deposition: Insights from In Situ Photoluminescence and X-ray Scattering. *ACS Appl. Mater. Interfaces* **2024**, *16* (27), 35723−35731.
(25) Held, V.; Mrkyvkova, N.; Nadazdy, P.; Vegso, K.; Vlk, A.; Ledinsky, M.; Jergel, M.; Chumakov, A.; Roth, S. V.; Schreiber, F.; Siffalovic, P. Evolution of Structure and Optoelectronic Properties During Halide Perovskite Vapor Deposition. *J. Phys. Chem. Lett.* **2022**, *13*, 11905.
(26) Schötz, K.; Panzer, F. Using in Situ Optical Spectroscopy to Elucidate Film Formation of Metal Halide Perovskites. *J. Phys. Chem. A* **2021**, *125*, 2209.
(27) Suchan, K.; Just, J.; Becker, P.; Unger, E. L.; Unold, T. Optical: In Situ Monitoring during the Synthesis of Halide Perovskite Solar Cells Reveals Formation Kinetics and Evolution of Optoelectronic Properties. *J. Mater. Chem. A Mater.* **2020**, *8* (20), 10439−10449.
(28) Song, T.-B.; Yuan, Z.; Babbe, F.; Nenon, D. P.; Aydin, E.; De Wolf, S.; Sutter-Fella, C. M. Dynamics of Antisolvent Processed Hybrid Metal Halide Perovskites Studied by In Situ Photoluminescence and Its Influence on Optoelectronic Properties. *ACS Appl. Energy Mater.* **2020**, *3* (3), 2386−2393.
(29) Song, T.-B.; Yuan, Z.; Mori, M.; Motiwala, F.; Segev, G.; Masquelier, E.; Stan, C. V.; Slack, J. L.; Tamura, N.; Sutter-Fella, C. M. Revealing the Dynamics of Hybrid Metal Halide Perovskite Formation via Multimodal In Situ Probes. *Adv. Funct Mater.* **2020**, *30* (6), 1908337.
(30) Guesnay, Q.; Sahli, F.; Artuk, K.; Turkay, D.; Kuba, A. G.; Mrkyvkova, N.; Vegso, K.; Siffalovic, P.; Schreiber, F.; Lai, H.; Fu, F.; Ledinský, M.; Fürst, N.; Schafflützel, A.; Bucher, C.; Jeangros, Q.; Ballif, C.; Wolff, C. M. Pizza Oven Processing of Organohalide Perovskites (POPOP): A Simple, Versatile and Efficient Vapor Deposition Method. *Adv. Energy Mater.* **2024**, *14* (10), 2303423.
(31) Kliner, V.; Soto-Montero, T.; Nespoli, J.; Savenije, T. J.; Ledinský, M.; Morales-Masis, M. Pulsed Laser Deposition of Halide Perovskites with over 10-Fold Enhanced Deposition Rates. *J. Phys. Chem. Lett.* **2025**, *16*, 1453−1460.
(32) Malinkiewicz, O.; Yella, A.; Lee, Y. H.; Espallargas, G. M.; Graetzel, M.; Nazeeruddin, M. K.; Bolink, H. J. Perovskite Solar Cells Employing Organic Charge-Transport Layers. *Nat. Photonics* **2014**, *8* (2), 128−132.
(33) Castro-Méndez, A. F.; Perini, C. A. R.; Hidalgo, J.; Ranke, D.; Vagott, J. N.; An, Y.; Lai, B.; Luo, Y.; Li, R.; Correa-Baena, J. P. Formation of a Secondary Phase in Thermally Evaporated MAPbI3and Its Effects on Solar Cell Performance. *ACS Appl. Mater. Interfaces* **2022**, *14*, 34269.
(34) Shao, Z.; You, S.; Guo, X.; Xiao, J.; Liu, J.; Song, F.; Xie, H.; Sun, J.; Huang, H. Temperature-Dependent Photoluminescence of Co-Evaporated MAPbI3 Ultrathin Films. *Results Phys.* **2022**, *34*, 105326.
(35) Parrott, E. S.; Patel, J. B.; Haghighirad, A. A.; Snaith, H. J.; Johnston, M. B.; Herz, L. M. Growth Modes and Quantum Confinement in Ultrathin Vapour-Deposited MAPbI3 Films. *Nanoscale* **2019**, *11* (30), 14276−14284.
(36) Palazon, F.; Pérez-del-Rey, D.; Dänekamp, B.; Dreessen, C.; Sessolo, M.; Boix, P. P.; Bolink, H. J. Room-Temperature Cubic Phase Crystallization and High Stability of Vacuum-Deposited Methylammonium Lead Triiodide Thin Films for High-Efficiency Solar Cells. *Adv. Mater.* **2019**, *31* (39), 1902692.
(37) Song, T.-B.; Yuan, Z.; Mori, M.; Motiwala, F.; Segev, G.; Masquelier, E.; Stan, C. V.; Slack, J. L.; Tamura, N.; Sutter-Fella, C. M. Revealing the Dynamics of Hybrid Metal Halide Perovskite Formation via Multimodal In Situ Probes. *Adv. Funct Mater.* **2020**, *30* (6), 1−11.
(38) Wagner, L.; Mundt, L. E.; Mathiazhagan, G.; Mundus, M.; Schubert, M. C.; Mastroianni, S.; Würfel, U.; Hinsch, A.; Glunz, S. W. Distinguishing Crystallization Stages and Their Influence on Quantum Efficiency during Perovskite Solar Cell Formation in Real-Time. *Sci. Rep* **2017**, *7* (1), 1−6.
(39) Giovanni, D. Optical-Spin Dynamics in Organic-Inorganic Lead Halide Perovskites, 2018. DOI: 10.13140/RG.2.2.35356.59523.
(40) De Wolf, S.; Holovsky, J.; Moon, S. J.; Löper, P.; Niesen, B.; Ledinsky, M.; Haug, F. J.; Yum, J. H.; Ballif, C. Organometallic Halide Perovskites: Sharp Optical Absorption Edge and Its Relation to Photovoltaic Performance. *J. Phys. Chem. Lett.* **2014**, *5* (6), 1035−1039.
(41) Stolterfoht, M.; Caprioglio, P.; Wolff, C. M.; Márquez, J. A.; Nordmann, J.; Zhang, S.; Rothhardt, D.; Hörmann, U.; Amir, Y.; Redinger, A.; Kegelmann, L.; Zu, F.; Albrecht, S.; Koch, N.; Kirchartz, T.; Saliba, M.; Unold, T.; Neher, D. The Impact of Energy Alignment and Interfacial Recombination on the Internal and External Open-Circuit Voltage of Perovskite Solar Cells. *Energy Environ. Sci.* **2019**, *12* (9), 2778−2788.
(42) Cao, J.; Tao, S. X.; Bobbert, P. A.; Wong, C. P.; Zhao, N. Interstitial Occupancy by Extrinsic Alkali Cations in Perovskites and Its Impact on Ion Migration. *Adv. Mater.* **2018**, *30* (26), 1−9.
(43) Li, W.; Zhan, J.; Liu, X.; Tang, J.; Yin, W. J.; Prezhdo, O. V. Atomistic Mechanism of Passivation of Halide Vacancies in Lead Halide Perovskites by Alkali Ions. *Chem. Mater.* **2021**, *33* (4), 1285−1292.
(44) Tang, Z.; Bessho, T.; Awai, F.; Kinoshita, T.; Maitani, M. M.; Jono, R.; Murakami, T. N.; Wang, H.; Kubo, T.; Uchida, S.; Segawa, H. Hysteresis-Free Perovskite Solar Cells Made of Potassium-Doped Organometal Halide Perovskite. *Sci. Rep* **2017**, *7* (1), 1−7.
(45) Wang, H.; Zou, W.; Ouyang, Y.; Liu, X.; Li, H.; Luo, H.; Zhao, X. Potassium Salt Coordination Induced Ion Migration Inhibition and Defect Passivation for High-Efficiency Perovskite Solar Cells. *J. Phys. Chem. Lett.* **2022**, *13* (36), 8573−8579.
(46) Zhang, J.; Cheng, N.; Zhou, H.; Zhong, J.; He, F.; Chen, Y.; Chen, C.; Liu, Z.; Zong, P. an. Dual-Sites Passivation for Efficient and

Stable Carbon-Based Perovskite Solar Cells. *Mater. Today Energy* **2024**, *43*, 101599.
(47) Yu, H.; Wang, F.; Xie, F.; Li, W.; Chen, J.; Zhao, N. The Role of Chlorine in the Formation Process of "CH3NH3PbI3-XClx" Perovskite. *Adv. Funct Mater.* **2014**, *24* (45), 7102−7108.
(48) Dastidar, S.; Egger, D. A.; Tan, L. Z.; Cromer, S. B.; Dillon, A. D.; Liu, S.; Kronik, L.; Rappe, A. M.; Fafarman, A. T. High Chloride Doping Levels Stabilize the Perovskite Phase of Cesium Lead Iodide. *Nano Lett.* **2016**, *16* (6), 3563−3570.
(49) Pramchu, S.; Cheiwchanchamnangij, T.; Laosiritaworn, Y.; Jaroenjittichai, A. P. Enhancing Surface Stabilization of CH3NH3PbI3 Perovskite by Cl and Br Doping: First-Principles Study. *J. Appl. Phys.* **2019**, *125* (11), 115302.
(50) Unger, E. L.; Bowring, A. R.; Tassone, C. J.; Pool, V. L.; Gold-Parker, A.; Cheacharoen, R.; Stone, K. H.; Hoke, E. T.; Toney, M. F.; McGehee, M. D. Chloride in Lead Chloride-Derived Organo-Metal Halides for Perovskite-Absorber Solar Cells. *Chem. Mater.* **2014**, *26* (24), 7158−7165.
(51) Nan, G.; Zhang, X.; Abdi-Jalebi, M.; Andaji-Garmaroudi, Z.; Stranks, S. D.; Lu, G.; Beljonne, D. How Methylammonium Cations and Chlorine Dopants Heal Defects in Lead Iodide Perovskites. *Adv. Energy Mater.* **2018**, *8* (13), 1−9.
(52) Shen, X.; Gallant, B. M.; Holzhey, P.; Smith, J. A.; Elmestekawy, K. A.; Yuan, Z.; Rathnayake, P. V. G. M.; Bernardi, S.; Dasgupta, A.; Kasparavicius, E.; Malinauskas, T.; Caprioglio, P.; Shargaieva, O.; Lin, Y. H.; McCarthy, M. M.; Unger, E.; Getautis, V.; Widmer-Cooper, A.; Herz, L. M.; Snaith, H. J. Chloride-Based Additive Engineering for Efficient and Stable Wide-Bandgap Perovskite Solar Cells. *Adv. Mater.* **2023**, *35* (30), 2211742.
(53) Li, H.; Zhou, J.; Tan, L.; Li, M.; Jiang, C.; Wang, S.; Zhao, X.; Liu, Y.; Zhang, Y.; Ye, Y.; Tress, W.; Yi, C. Sequential Vacuum-Evaporated Perovskite Solar Cells with More than 24% Efficiency. *Sci. Adv.* **2022**, *8* (28), 1−8.
(54) Weller, M. T.; Weber, O. J.; Henry, P. F.; Di Pumpo, A. M.; Hansen, T. C. Complete Structure and Cation Orientation in the Perovskite Photovoltaic Methylammonium Lead Iodide between 100 and 352 K. *Chem. Commun.* **2015**, *51*, 4180−4183.
(55) Baikie, T.; Fang, Y.; Kadro, J. M.; Schreyer, M.; Wei, F.; Mhaisalkar, S. G.; Graetzel, M.; White, T. J. Synthesis and Crystal Chemistry of the Hybrid Perovskite (CH 3NH3)PbI3 for Solid-State Sensitised Solar Cell Applications. *J. Mater. Chem. C Mater.* **2013**, *1* (18), 5628−5641.
(56) Stoumpos, C. C.; Malliakas, C. D.; Kanatzidis, M. G. Semiconducting Tin and Lead Iodide Perovskites with Organic Cations: Phase Transitions, High Mobilities, and Near-Infrared Photoluminescent Properties. *Inorg. Chem.* **2013**, *52*, 9019−9038.
(57) Mrkyvkova, N.; Held, V.; Halahovets, Y.; Nádaždy, P.; Jergel, M.; Majková, E.; Schreiber, F.; Siffalovic, P. Simultaneous Measurement of X-Ray Scattering and Photoluminescence during Molecular Deposition. *J. Lumin.* **2022**, *248*, 118950.
(58) Park, B.; Kedem, N.; Kulbak, M.; Lee, D. Y.; Yang, W. S.; Jeon, N. J.; Seo, J.; Kim, G.; Kim, K. J.; Shin, T. J.; Hodes, G.; Cahen, D.; Seok, S. Il. Understanding How Excess Lead Iodide Precursor Improves Halide Perovskite Solar Cell Performance. *Nat. Commun.* **2018**, *9* (1), 3301.
(59) Liang, Q.; Han, J.; Li, H.; Chen, L.; Xie, Z.; Liu, J.; Han, Y. Uniform, High Crystalline, (100) Crystal Orientated Perovskite Films without PbI_2 Residue by Controlling the Nanostructure of PbI_2. *Org. Electron* **2018**, *53*, 26−34.
(60) Xiong, Z.; Chen, X.; Zhang, B.; Odunmbaku, G. O.; Ou, Z.; Guo, B.; Yang, K.; Kan, Z.; Lu, S.; Chen, S.; Ouedraogo, N. A. N.; Cho, Y.; Yang, C.; Chen, J.; Sun, K. Simultaneous Interfacial Modification and Crystallization Control by Biguanide Hydrochloride for Stable Perovskite Solar Cells with PCE of 24.4%. *Adv. Mater.* **2022**, *34* (8), 2106118.
(61) Fu, L.; Li, H.; Wang, L.; Yin, R.; Li, B.; Yin, L. Defect Passivation Strategies in Perovskites for an Enhanced Photovoltaic Performance. *Energy Environ. Sci.* **2020**, *13* (11), 4017−4056.
(62) Euvrard, J.; Gunawan, O.; Mitzi, D. B. Impact of PbI2 Passivation and Grain Size Engineering in CH3NH3PbI3 Solar Absorbers as Revealed by Carrier-Resolved Photo-Hall Technique. *Adv. Energy Mater.* **2019**, *9* (47), 1902706.
(63) Nandi, P.; Giri, C.; Joseph, B.; Rath, S.; Manju, U.; Topwal, D. CH3NH3PbI3, A Potential Solar Cell Candidate: Structural and Spectroscopic Investigations. *J. Phys. Chem. A* **2016**, *120* (49), 9732−9739.
(64) Tombe, S.; Adam, G.; Heilbrunner, H.; Apaydin, D. H.; Ulbricht, C.; Sariciftci, N. S.; Arendse, C. J.; Iwuoha, E.; Scharber, M. C. Optical and Electronic Properties of Mixed Halide (X = I, Cl, Br) Methylammonium Lead Perovskite Solar Cells. *J. Mater. Chem. C Mater.* **2017**, *5* (7), 1714−1723.
(65) Segovia, R.; Ding, L.; Jiang, H.; Miao, P.; Sun, X.; Shi, H.; Gao, B. Effect of Phase Transition Stress on the Photoluminescence of Perovskite CH3NH3PbI3Microwires. *J. Mater. Sci.* **2019**, *54* (7), 5331−5342.
(66) Bommel, S.; Kleppmann, N.; Weber, C.; Spranger, H.; Schäfer, P.; Novak, J.; Roth, S. V.; Schreiber, F.; Klapp, S. H. L.; Kowarik, S. Unravelling the Multilayer Growth of the Fullerene C 60 in Real Time. *Nat. Commun.* **2014**, *5* (5388), 1−8.
(67) Schwartzkopf, M.; Buffet, A.; Körstgens, V.; Metwalli, E.; Schlage, K.; Benecke, G.; Perlich, J.; Rawolle, M.; Rothkirch, A.; Heidmann, B.; Herzog, G.; Müller-Buschbaum, P.; Röhlsberger, R.; Gehrke, R.; Stribeck, N.; Roth, S. V. From Atoms to Layers: In Situ Gold Cluster Growth Kinetics during Sputter Deposition. *Nanoscale* **2013**, *5* (11), 5053−5062.
(68) Santoro, G.; Yu, S. Grazing Incidence Small Angle X-Ray Scattering as a Tool for In- Situ Time-Resolved Studies. In *X-ray Scattering*; Ares, A. E., Ed.; IntechOpen: 2017. DOI: 10.5772/64877.